Tunable helical ribbons

Z. Chen,[1,2] C. Majidi,[3] D. J. Srolovitz,[4] and M. Haataja[1,2,5,a)]
[1]*Department of Mechanical and Aerospace Engineering, Princeton University, Princeton, New Jersey 08544, USA*
[2]*Princeton Institute for the Science and Technology of Materials (PRISM), Princeton University, Princeton, New Jersey 08544, USA*
[3]*School of Engineering and Applied Sciences, Harvard University, Cambridge, Massachusetts 02138, USA*
[4]*Institute of High Performance Computing, 1 Fusionopolis Way, Singapore 138632*
[5]*Program in Applied and Computational Mathematics (PACM), Princeton University, Princeton, New Jersey 08544, USA*

(Received 20 October 2010; accepted 2 December 2010; published online 5 January 2011)

The helix angle, chirality, and radius of helical ribbons are predicted with a comprehensive, three-dimensional analysis that incorporates elasticity, differential geometry, and variational principles. In many biological and engineered systems, ribbon helicity is commonplace and may be driven by surface stress, residual strain, and geometric or elastic mismatch between layers of a laminated composite. Unless coincident with the principle geometric axes of the ribbon, these anisotropies will lead to spontaneous, three-dimensional helical deformations. Analytical, closed-form ribbon shape predictions are validated with table-top experiments. More generally, our approach can be applied to develop materials and systems with tunable helical geometries. © *2011 American Institute of Physics*. [doi:10.1063/1.3530441]

Helical ribbons represent an important class of two-dimensional structures that often arise in biology[1,2] and engineering.[3–6] They exhibit unique shapes that cannot be sufficiently described with one-dimensional theories of helicity that are commonly applied to nonribbonlike structures such as DNA and mechanical springs[7] or with classical Stoney/Timoshenko approaches that are routinely applied to beam/planar structures.[8–11] A predictive model for the mechanics and morphological stability of helical ribbons represents a new and important tool for study and design in such diverse technologies as drug delivery and biosensing,[12,13] nanoengineered helices for optoelectronics,[14] and microrobotics.[15]

Typically, ribbon helicity is controlled by the balance of surface stress or internal residual stress with restoring forces induced by elastic stretching and bending. For quaternary sterol solutions such as model bile, residual stress may be induced by a mismatch in molecular packing between constituent layers,[12] while for nanoengineered helices, deformation is usually driven by epitaxial strains.[14] Moreover, at least one of these mechanical elements (surface stress,[16] residual strain, and elastic modulus[4]) must be anisotropic and have a principle orientation that does not coincide with the principle geometric axes (length, width, and thickness) of the ribbon.

In this paper, we use elasticity theory, differential geometry, and stationarity principles to predict the shape of helical ribbons subject to either surface stress or residual strain. The analytic predictions are in closed-form and are validated with simple, table-top experiments in which layers of prestretched elastic sheets are bonded together to form a laminated ribbon. The analysis identifies unique, mechanically stable morphologies that cannot be explained with classical rod or plate theories.

a)Electronic mail: mhaataja@princeton.edu.

In our work, the ribbon is defined as an elastic sheet with length L, width $w \ll L$, and thickness $H \ll w$. The ribbon has a rectangular cross-section and principle geometric axes along its length ($\mathbf{d}_x$), width ($\mathbf{d}_y$), and thickness ($\mathbf{d}_z$). These directions form an orthonormal triad of directors $\{\mathbf{d}_x, \mathbf{d}_y, \mathbf{d}_z\}$ that rotate with the ribbon as it bends and twists in space.

In the special case of planar bending, as is assumed in the Stoney formula,[8] curvature is restricted to the (lengthwise) $\mathbf{d}_x$ direction. For a helical ribbon, however, the ribbon will have principle curvatures κ_1 and κ_2 along the directors $\mathbf{r}_1 = \cos\phi\,\mathbf{d}_x - \sin\phi\,\mathbf{d}_y$ and $\mathbf{r}_2 = \sin\phi\,\mathbf{d}_x + \cos\phi\,\mathbf{d}_y$ oriented at an angle ϕ relative to $\mathbf{d}_x$ within the plane of the ribbon—see Fig. 1.

In a global Cartesian coordinate system, the $\{X, Y, Z\}$ coordinates of a point P on the centerline can be parametrized by the arclength s via $X(s) = s - \beta^2/\alpha^3(\alpha s - \sin\alpha s)$, $Y(s) = \beta/\alpha^3(\alpha s - \sin\alpha s)(\kappa_1 - \kappa_2)\sin\phi\cos\phi$, and $Z(s) = \beta/\alpha^2(\cos\alpha s - 1)$, where $\alpha = \sqrt{\kappa_1^2\cos^2\phi + \kappa_2^2\sin^2\phi}$ and $\beta = \kappa_1\cos^2\phi + \kappa_2\sin^2\phi$.

In the presence of anisotropic bending curvatures, the ribbon is subject to strains ϵ_{xx}, ϵ_{yy}, ϵ_{xy}, and ϵ_{zz} that are considered uniform throughout the $\mathbf{d}_y$ direction of the ribbon

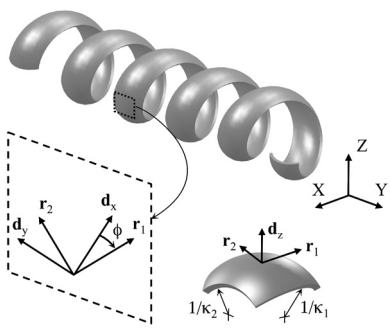

FIG. 1. Illustration of a helical ribbon. The directors $\mathbf{d}_x$ and $\mathbf{d}_y$ are oriented along the length and widthwise axes of the ribbon, respectively. The bases $\mathbf{r}_1$ and $\mathbf{r}_2$ correspond to the principle directions of curvature.

(assuming that the thickness w is relatively small compared to the radii of curvature). Superimposing these yields a strain tensor $\boldsymbol{\gamma}=\gamma_{ij}\mathbf{d}_i\otimes\mathbf{d}_j(i,j\in\{x,y,z\})$ with components $\gamma_{xx}=\epsilon_{xx}+z(\kappa_1\cos^2\phi+\kappa_2\sin^2\phi)+\gamma^0_{xx}(z)$, $\gamma_{xy}=\epsilon_{xy}+z(\kappa_2-\kappa_1)\sin\phi\cos\phi+\gamma^0_{xy}(z)$, $\gamma_{yy}=\epsilon_{yy}+z(\kappa_1\sin^2\phi+\kappa_2\cos^2\phi)+\gamma^0_{yy}(z)$, and $\gamma_{zz}=\epsilon_{zz}+zk_3+\gamma^0_{zz}(z)$. Here, $z\in[-H/2,H/2]$ denotes the distance from the ribbon midplane, while $\gamma^0_{ij}(z)$ denotes an arbitrary residual strain within the (initially) flat ribbon.

Let ϕ^+ and ϕ^- denote the orientation of the principle axes of surface stress on the $z=H/2$ and $z=-H/2$ surfaces, respectively. In contrast to ϕ, which is an unknown, both ϕ^+ and ϕ^- are predetermined by nature or during fabrication (e.g., the principle axes of the surface stress tensor, $\mathbf{f}$). On the $z=\pm H/2$ surfaces, $\mathbf{f}$ has the form $\mathbf{f}^\pm=f^\pm_1\mathbf{e}^\pm_1\otimes\mathbf{e}^\pm_1+f^\pm_2\mathbf{e}^\pm_2\otimes\mathbf{e}^\pm_2$, where $\mathbf{e}^\pm_1=\cos\phi^\pm\mathbf{d}_x-\sin\phi^\pm\mathbf{d}_y$ and $\mathbf{e}^\pm_2=\sin\phi^\pm\mathbf{d}_x+\cos\phi^\pm\mathbf{d}_y$. The potential energy density of the ribbon is

$$\Pi=\mathbf{f}^-:\boldsymbol{\gamma}|_{z=-H/2}+\mathbf{f}^+:\boldsymbol{\gamma}|_{z=H/2}+\int_{-H/2}^{H/2}\frac{1}{2}\boldsymbol{\gamma}:\mathbf{C}:\boldsymbol{\gamma}dz, \tag{1}$$

where $\mathbf{C}$ is the fourth-order elastic constant tensor. It is important to note that for an elastically anisotropic ribbon, the principle bases of $\mathbf{C}$ may not coincide with $\{\mathbf{d}_x,\mathbf{d}_y,\mathbf{d}_z\}$. At equilibrium, Π must be stationary with respect to the unknown parameters κ_1, κ_2, k_3, ϵ_{xx}, ϵ_{yy}, ϵ_{xy}, ϵ_{zz}, and ϕ. That is, these values are the solutions to a set of linearly independent equations $\partial\Pi/\partial\chi=0$, where χ represents any one of the eight unknowns. These solutions exist for arbitrary anisotropic elastic constant tensor, residual strains, and surface stresses on the two surfaces. However, such solutions can either be very long or can only be evaluated numerically. We therefore focus on a small set of interesting cases below.

A closed-form analytic solution can be obtained for the special case of a homogeneous, elastically isotropic ribbon with surface stresses on either one or two surfaces and no internal residual strain. First, we consider a surface stress only on the $z=-H/2$ surface of the form $\mathbf{f}^-=f^-_1\mathbf{e}^-_1\otimes\mathbf{e}^-_1+f^-_2\mathbf{e}^-_2\otimes\mathbf{e}^-_2$. The strain tensor is diagonalized in the orthogonal coordinate system $(\mathbf{e}^-_1,\mathbf{e}^-_2,\mathbf{d}_z)$ such that the only nonzero strain components are $\gamma_{11}=\epsilon_{11}+z\kappa_1$, $\gamma_{22}=\epsilon_{22}+z\kappa_2$, and $\gamma_{33}=\epsilon_{33}+zk_3$. The total potential energy is

$$\begin{aligned}\Pi=&\frac{EH^3}{24}\left[\frac{\nu(\kappa_1+\kappa_2+k_3)^2}{(1-2\nu)(1+\nu)}+\frac{(\kappa_1^2+\kappa_2^2+k_3^2)}{1+\nu}\right]H^3\\&+\frac{EH}{2}\left[\frac{\nu(\epsilon_{11}+\epsilon_{22}+\epsilon_{33})^2}{(1-2\nu)(1+\nu)}+\frac{(\epsilon_{11}^2+\epsilon_{22}^2+\epsilon_{33}^2)}{1+\nu}\right]\\&+[f^-_1\cos^2(\phi-\phi^-)+f^-_2\sin^2(\phi-\phi^-)]\left(\epsilon_{11}-\frac{\kappa_1H}{2}\right)\\&+[f^-_1\sin^2(\phi-\phi^-)+f^-_2\cos^2(\phi-\phi^-)]\left(\epsilon_{22}-\frac{\kappa_2H}{2}\right).\end{aligned} \tag{2}$$

Applying the stationary conditions implies that the principle directions of the curvature and surface stress coincide, i.e., $\phi=\phi^-$, and that

$$\kappa_1=\frac{6(f^-_1-\nu f^-_2)}{EH^2},\quad \kappa_2=\frac{6(f^-_2-\nu f^-_1)}{EH^2},$$

$$k_3=-\frac{6\nu(f^-_1+f^-_2)}{EH^2},\quad \epsilon_{11}=-\frac{f^-_1-\nu f^-_2}{EH},$$

$$\epsilon_{22}=-\frac{f^-_2-\nu f^-_1}{EH},\quad \epsilon_{33}=\frac{\nu(f^-_1+f^-_2)}{EH}. \tag{3}$$

Here, E and ν denote the Young's modulus and Poisson's ratio, respectively. It is interesting to note that in the absence of Poisson coupling, the first two equations reduce to the Stoney formula in the two principle directions of curvature: $\kappa_1=6f^-_1/EH^2$ and $\kappa_2=6f^-_2/EH^2$.

More generally, given surface stresses $\mathbf{f}^+$ and $\mathbf{f}^-$ on the top and bottom surfaces, respectively, we define the stretching component of the surface stress $\mathbf{f}^s\equiv\mathbf{f}^++\mathbf{f}^-$ and the bending component $\mathbf{f}^*\equiv\mathbf{f}^--\mathbf{f}^+$. Here, $\mathbf{f}^*$ is treated as the effective stress acting on the bottom $(z=-H/2)$ surface. Next, $\mathbf{f}^s$ and $\mathbf{f}^*$ are diagonalized with respect to principle axes $(\mathbf{u}_1,\mathbf{u}_2)$ and $(\mathbf{r}_1,\mathbf{r}_2)$: $\mathbf{f}^s=f^s_1\mathbf{u}_1\otimes\mathbf{u}_1+f^s_2\mathbf{u}_2\otimes\mathbf{u}_2$ and $\mathbf{f}^*=f^*_1\mathbf{r}_1\otimes\mathbf{r}_1+f^*_2\mathbf{r}_2\otimes\mathbf{r}_2$. By decoupling the stretching and bending modes and applying stationarity principles, we obtain the total strain $\boldsymbol{\gamma}=\boldsymbol{\gamma}_s+\boldsymbol{\gamma}_b$, where $\boldsymbol{\gamma}_s=-(f^s_1-\nu f^s_2)/(EH)\mathbf{u}_1\otimes\mathbf{u}_1-(f^s_2-\nu f^s_1)/(EH)\mathbf{u}_2\otimes\mathbf{u}_2$ is the strain due to stretching and $\boldsymbol{\gamma}_b=\kappa_1z\mathbf{r}_1\otimes\mathbf{r}_1+\kappa_2z\mathbf{r}_2\otimes\mathbf{r}_2+k_3z\mathbf{d}_z\otimes\mathbf{d}_z$ is the strain caused by effective surface stress on the bottom surface. Here $\kappa_1=6(f^*_1-\nu f^*_2)/EH^2$, $\kappa_2=6(f^*_2-\nu f^*_1)/EH^2$, and $k_3=-6\nu(f^*_1+f^*_2)/EH^2$.

The helix angle Φ, radius R, and chirality of the helix (see Fig. 1) are determined from the values of κ_1, κ_2, and ϕ obtained from the analysis. More specifically, the helix angle between the central axis of the bounding cylinder and the widthwise axis $(\mathbf{d}_y)$ of the ribbon is

$$\Phi=\arctan\frac{(\kappa_1-\kappa_2)\sin\phi\cos\phi}{\kappa_1\cos^2\phi+\kappa_2\sin^2\phi}. \tag{4}$$

Moreover, the centerline of the ribbon wraps around a bounding cylinder of radius

$$R=\frac{\kappa_1\cos^2\phi+\kappa_2\sin^2\phi}{\kappa_1^2\cos^2\phi+\kappa_2^2\sin^2\phi}. \tag{5}$$

The chirality of the helix is determined by the sign of the helix angle (or equivalently the torsion of the ribbon centerline), i.e., $\mathrm{sgn}(\Phi)$. Right-handed helices correspond to $\Phi>0$, whereas left-handed helices correspond to $\Phi<0$. According to Eq. (4), the chirality is determined by the signs of both $(\kappa_1-\kappa_2)$ and $\sin\phi\cos\phi$.

The ribbon forms a ring when either $\kappa_1=\kappa_2$, $\phi=0$, or $\phi=\pi/2$. For zero Gaussian curvature, i.e., when either κ_1 or κ_2 is zero, the ribbon bend into a cylindrical shape. Also, when $\kappa_2=-\kappa_1$ and $\phi=\pi/4$, the mean curvature $(\kappa_1+\kappa_2)/2$ vanishes and the ribbon undergoes a pure twist deformation (i.e., the centerline remains straight).

To verify these predictions, we performed a series of simple, table-top experiments. A sheet of latex rubber was prestretched and bonded to an elastic strip of thick, pressure-sensitive adhesive.[17] Helical ribbons with different helix angle, helical radius, chirality, and Gaussian curvature were obtained by altering the magnitudes of the two principle prestretches and their angle with respect to the centerline orientation of the bonded strip (as described in the caption of Fig. 2). As shown in Fig. 2, the theoretical predictions for helix angle and ribbon shape are in excellent agreement with experimental observations. Validation of the theory is also

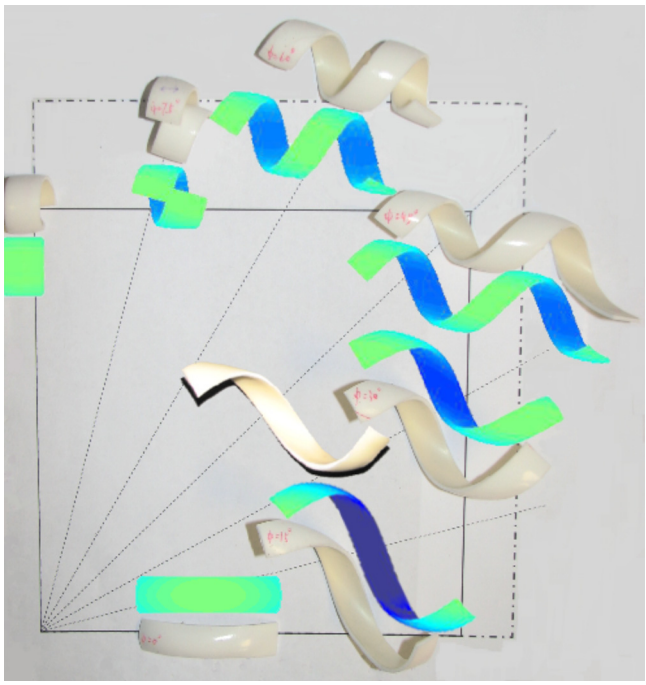

FIG. 2. (Color online) A square piece of latex rubber (solid lines) is stretched twice as much in the vertical direction than in the horizontal direction (dashed-dotted edges). An unstrained elastic adhesive sheet is then bonded to the strained latex sheet and subsequently cut into ribbons with long axis varying between 0° and 90° (15° intervals). The released samples are shown at the appropriate angles along with the corresponding theoretical prediction. The ribbon at the center is composed of prestretched top (pure horizontal) and bottom (twice the stretch, biaxial) layers with long axis orientation ϕ=30°. As predicted, the stationary configuration is similar to a ribbon with prestretch only on the bottom surface.

demonstrated for the more general case in which both sides of the elastic strip are bonded to prestretched layers of latex rubber. More specifically, a ribbon composed of prestretched top (pure horizontal) and bottom (twice the stretch, biaxial) layers was cut along the long axis orientation ϕ=30°. According to the theory, the resulting helical shape should be identical to the one obtained from a single prestretched layer stretched twice as much in the vertical direction than in the horizontal direction and subsequently cut along the same long axis orientation (ϕ=30°). Indeed, our experiments are consistent with this prediction, as illustrated in Fig. 2.

The central result of the present work is the development of a three-dimensional solution (based on continuum elasticity, differential geometry, and stationarity principles) for the shape of an initially flat, straight ribbon deformed into a helical form (including curvature parallel and perpendicular to the major and secondary axes) when subject to arbitrary surface stress and/or internal residual strain distribution. It establishes the relationship between surface stress, residual strain, elasticity, helix angle, helix radius, and chirality. The present results represent a new formalism for predicting the shape of helical structures and for tuning the design of ribbons with desirable geometric properties for use in a broad spectrum of biological and engineering applications.

This work has been in part supported by the NSF-DMR Grant No. DMR-0449184 (M.H.).

[1]D. S. Chung, G. B. Benedek, F. M. Konikoff, and J. M. Donovan, Proc. Natl. Acad. Sci. U.S.A. **90**, 11341 (1993).
[2]R. L. B. Selinger, J. V. Selinger, A. P. Malanoski, and J. M. Schnur, Phys. Rev. Lett. **93**, 158103 (2004).
[3]X. Y. Kong and Z. L. Wang, Nano Lett. **3**, 1625 (2003).
[4]L. Zhang, E. Deckhardt, A. Weber, C. Schönenberger, and D. Grützmacher, Nanotechnology **16**, 655 (2005).
[5]A. Cho, Science **313**, 164 (2006).
[6]S. Srivastava, A. Santos, K. Critchley, K.-S. Kim, P. Podsiadlo, K. Sun, J. Lee, C. Xu, G. D. Lilly, S. C. Glotzer, and N. A. Kotov, Science **327**, 1355 (2010).
[7]N. Chouaieb, A. Goriely, and J. H. Maddocks, Proc. Natl. Acad. Sci. U.S.A. **103**, 9398 (2006).
[8]G. G. Stoney, Proc. R. Soc. London, Ser. A **82**, 172 (1909).
[9]S. Timoshenko, J. Opt. Soc. Am. **11**, 233 (1925).
[10]Z. Suo, E. Y. Ma, H. Gleskova, and S. Wagner, Appl. Phys. Lett. **74**, 1177 (1999).
[11]J. Zang, M. Huang, and F. Liu, Phys. Rev. Lett. **98**, 146102 (2007).
[12]Y. V. Zastavker, N. Asherie, A. Lomakin, J. Pande, J. M. Donovan, J. M. Schnur, and G. B. Benedek, Proc. Natl. Acad. Sci. U.S.A. **96**, 7883 (1999).
[13]B. Smith, Y. V. Zastaver, and G. B. Benedek, Phys. Rev. Lett. **87**, 278101 (2001).
[14]G. Hwang, C. Dockendorf, D. Bell, L. Dong, H. Hashimoto, D. Poulikakos, and B. Nelson, Int. J. Optomechatronics **2**, 88 (2008).
[15]J. J. Abbott, K. E. Peyer, M. C. Lagomarsino, L. Zhang, L. Dong, I. K. Kaliakatsos, and B. J. Nelson, Int. J. Robot. Res. **28**, 1434 (2009).
[16]J. Wang, X. Feng, G. Wang, and S. Yu, Appl. Phys. Lett. **92**, 191901 (2008).
[17]The latex sheets were produced by Small Parts Inc. and the elastic strips were acrylic, scotch wall-mounting tape, produced by 3*M*. Their Young's moduli are 1.4 and 10.3 MPa, respectively, measured by Instron™ 5848 micro-tester. The Poisson's ratio of acrylic is taken to be 0.37 from biomaterials database at University of Michigan and is 0.49 for latex sheets [from Comput. Struct. **81**, 715 (2003)].